Radiation Physics and Chemistry 221 (2024) 111773

Contents lists available at ScienceDirect

Radiation Physics and Chemistry

journal homepage: www.elsevier.com/locate/radphyschem

Radiation exposure of patients from computed tomography for COVID-19 diagnosis

Daniel Lee [a], Jae Won Jung [b,*]

[a] Thomas S. Wootton High School, Rockville, MD, 20850, USA
[b] Department of Radiation Oncology, East Carolina University, Greenville, NC, 27858, USA

ARTICLE INFO

Handling Editor: Dr. Chris Chantler

Keywords:
COVID-19
Computed tomography
CTDI
Organ dose
Effective dose

ABSTRACT

Background: During the global Coronavirus Disease 2019 (COVID-19) pandemic, numerous computed tomography (CT) scans were conducted to assess pulmonary abnormalities associated with COVID-19. A number of studies have contributed to our current understanding of radiation doses in the context of chest CT scans for COVID-19 diagnosis, but there remains a discernible gap in the literature regarding organ-level dose assessments.
Materials and methods: We estimated organ and effective dose for the COVID-19-related chest CT patients in the following three steps. First, we collected $CTDI_{vol}$ and DLP from the literature published during and after COVID-19 pandemic period. Second, we developed the probability density functions (PDFs) for the $CTDI_{vol}$ and the starting location of CT scans by age groups from which 1000 sets of patient and technique parameters were created. With CT organ dose calculation software, National Cancer Institute dosimetry system for CT (NCICT), we calculated 1000 sets of plausible organ and effective doses and evaluated summary statistics for the patient population.
Results: The standard dose protocol administered approximately five times higher $CTDI_{vol}$ (5.4 mGy) to patients undergoing COVID-19-related chest CT scans compared to the low dose protocol (1.1 mGy). The median lung dose (11.8 mGy) for the 1-year-old patients was about 1.5 times greater than that (7.8 mGy) of the adult patients. We found that 75% of whole COVID-19-related CT patients would have received effective doses less than 6.4 mSv and 1.5 mSv when scanned by standard dose and low dose protocols, respectively.
Conclusion: We evaluated the distribution of organ and effective dose for the COVID-19-related chest CT patients worldwide by collecting comprehensive data of $CTDI_{vol}$ for the COVID-19-related chest CT scans from the literature and combining them with NCICT organ dose calculator. While past studies have predominantly reported basic CT dose descriptors, our work takes it a step further by reporting organ-level doses and effective doses. Subsequent research endeavors could involve enhancing the precision of radiation dose assessment through the collection of a subset of electronic CT records.

1. Introduction

During the global Coronavirus Disease 2019 (COVID-19) pandemic, numerous computed tomography (CT) scans were conducted to assess pulmonary abnormalities associated with COVID-19 (Homayounieh et al., 2020). Although major health and radiology organizations do not recommend the sole use of CT scans for the diagnosis of COVID-19 without reverse transcription polymerase chain reaction assay or antigen tests, a substantial portion of the hospitals worldwide used chest CT scans as the preferred testing method. While the diagnostic benefits of CT imaging are well-established, there is growing evidence regarding the associated radiation dose and its long term adverse effects for patient health (Bosch De Basea Gomez et al., 2023; Hauptmann et al., 2023; Pearce et al., 2012). Thus, healthcare professionals strive to strike a delicate balance between accurate diagnosis and minimizing unnecessary radiation exposure. Following two years of the COVID-19 pandemic, there is an immediate need to examine the radiation dose implications for the patient population that has undergone chest CT scans for COVID-19 diagnosis.

A number of studies have contributed to our current understanding of radiation doses in the context of chest CT scans for COVID-19 diagnosis, with a focus on reporting major CT dose descriptors such as the

* Corresponding author.
E-mail address: k311jjw@gmail.com (J.W. Jung).

https://doi.org/10.1016/j.radphyschem.2024.111773
Received 7 December 2023; Received in revised form 25 March 2024; Accepted 14 April 2024
Available online 15 April 2024

volumetric Computed Tomography Dose Index ($CTDI_{vol}$) and the Dose-Length Product (DLP). Investigations into these widely recognized dose metrics have provided essential baseline data, characterizing the level of overall radiation exposure for the CT scan procedure. While these studies have been instrumental in establishing general benchmarks for radiation exposure during COVID-19-related CT scans, those dose descriptors are measured using simple cylindrical phantoms with the uniform diameters of 16 or 32 cm, called CTDI phantoms, which do not directly represent dose delivered to patients' anatomy. There remains a discernible gap in the literature regarding organ-level dose assessments for COVID-19-related CT scans.

Recognizing the need to delve deeper into this critical aspect of radiation safety, in the current study, we evaluated major organ doses estimated to be delivered to patients who underwent chest CT scans for COVID-19 diagnosis. Since it requires a large scale global survey to obtain CT dose descriptors from hospitals, we established a comprehensive database of basic dose descriptors from the literature. We then calculated 1000 sets of plausible organ doses and effective doses for the patient cohort in various age groups by using an uncertainty propagation technique combined with a CT organ dose calculation tool. We provided the summary statistics of organ-level and effective doses for the patient population worldwide who underwent chest CT scans for COVID-19 diagnosis.

2. Materials and methods

We estimated organ and effective dose for the COVID-19-related chest CT patients in the following three steps. First, we collected $CTDI_{vol}$ and DLP from the literature published during and after COVID-19 pandemic period. Second, we developed the probability density functions (PDFs) for the $CTDI_{vol}$ and the starting location of CT scans by age groups from which 1000 sets of patient and technique parameters were created. With CT organ dose calculation software, National Cancer Institute dosimetry system for CT (NCICT) (Lee et al., 2022), we calculated 1000 sets of plausible organ and effective doses and evaluated summary statistics for the patient population.

2.1. Collection of CT dose descriptors

We searched scientific articles reporting CT dose descriptors for patients who underwent CT scans for COVID-19 diagnosis. From PubMed (https://pubmed.ncbi.nlm.nih.gov/), the keyword, "COVID19 chest CT dose" resulted in 218 articles published between 2020 and 2023. We only selected 30 articles containing $CTDI_{vol}$ or DLP or both. We gathered the mean, standard deviation, minimum, and maximum values of $CTDI_{vol}$ (mGy) and DLP (mGy-cm) manually from the chosen articles, to the extent that the information was accessible.

Many papers report the type of scan protocols: standard dose protocol, low dose protocol, and ultra low dose protocol. Since only a small number of articles report ultra low dose protocol, we combined the low dose and ultra low dose protocols into a single category, "low dose protocol." When scan protocols were not specified, we assumed that standard dose protocol was used when $CTDI_{vol}$ was greater than 3 mGy, which is recommended in low dose CT scans for lung cancer screening by the US Centers for Medicare & Medicaid Services.[1] We summarized $CTDI_{vol}$ and DLP into the two protocol categories: standard dose and low dose protocols. When both CTDI and DLP are available, we derived scan length (cm) using the following equation:

$$scan\ length\ (cm) = DLP(mGy \cdot cm)/CTDI_{vol}(mGy) \quad (1)$$

When $CTDI_{vol}$ is available but DLP is not, we derived DLP by multiplying $CTDI_{vol}$ with the average scan length. When DLP is available but $CTDI_{vol}$ is not, we derived $CTDI_{vol}$ by dividing DLP by the average scan length. Overbeaming may impact scan ranges derived from this relationship mentioned above. However, it is impossible to quantify the range of overbeaming around the penumbra based on the information collected from the literature. Its impact was assumed to be negligible for modern scanners with multi-section CT scanners (Goo, 2012). The age of patients in most articles is not explicitly stated, except in a few instances where adults over 40 years old were specifically included in the studies. It was also difficult to ascertain the dimensions of the CTDI phantom (16 or 32 cm) used for the reported CTDIvol values. We assumed all $CTDI_{vol}$ used for the COVID-19-related chest CT patients were based on a 32 cm body CTDI phantom for both pediatric and adult patients. Since most of the articles specified countries, we tabulated the data by country and derived national median values for comparison. We also derived minimum, Q1, median, Q3, and maximum values for $CTDI_{vol}$, DLP, and scan lengths after combining all country-specific data.

We then created the two probability density functions (PDF) representing the distribution of $CTDI_{vol}$ for the standard dose protocol and low dose protocol, respectively. Since a small number of data was available for some countries, we combined the data from all countries into the PDFs.

2.2. Scan locations

Next to the variation of $CTDI_{vol}$ impacting organs and effective doses, scan locations are also reported to be substantially affecting organ doses (Lee et al., 2019). As described above, when both $CTDI_{vol}$ and DLP were available, we derived scan length from those values. For the anatomical locations of scan start and end, we adopted the standard scan protocols for chest CT used at the National Institutes of Health Clinical Center (Lee et al., 2015): from the clavicles to the middle of the liver. The age-dependent scan coverage for chest CT that was used in the current study is presented for the five computational human phantoms of 1, 5, 10, 15 years and adult in Fig. 1. Scan start locations are presented in Fig. 1 as red lines with the distance from the top of the phantom's head presented on the left of each phantom: 20 cm (1 year), 23 cm (5 year), 25 cm (10 year), 28 cm (15 year), and 28 cm (adult).

We created a uniform distribution range above and below the scan start location by 5% of the phantom's height. For the adult phantom, for example, we assumed the range of scan start location as 28 cm ± 8.8 cm (the height of the adult male phantom, 176 cm x 0.05 = 8.8 cm). We randomly sampled a scan start location and derived the scan end location by adding the average scan range to the scan start location (i.e., scan end location = scan start location +average scan length). Sampled scan coverage and CTDIvol were then used for organ dose calculations as described below.

2.3. Organ and effective dose calculation

We adopted the NCICT version 3.0.20230428 (Lee et al., 2015, 2022) for organ and effective dose calculations. The program is designed to calculate organ-specific doses and effective doses by utilizing computational voxel phantoms representing reference individuals at different developmental stages. These phantoms are in accordance with the age categories defined by the International Commission on Radiological Protection (ICRP) (ICRP, 2020, 2010). The list of organs to which dose is calculated from NCICT includes: brain, pituitary gland, lens, eye balls, salivary glands, oral cavity, spinal cord, thyroid, esophagus, trachea, thymus, lungs, breast, heart wall, stomach wall, liver, gallbladder, adrenals, spleen, pancreas, kidney, small intestine, colon, rectosigmoid, urinary bladder, prostate, uterus, testes, ovaries, skin, muscle, active marrow, and shallow marrow.

NCICT requires the following input parameters for organ dose calculations: scan start (the distance of scan start location from the top of the patient in cm), scan end (the distance of scan end location from the top of the patient in cm), phantom group number (1 = pediatric female,

[1] https://www.cms.gov/medicare-coverage-database/view/ncacal-decision-memo.aspx?proposed=N&NCAId=274.

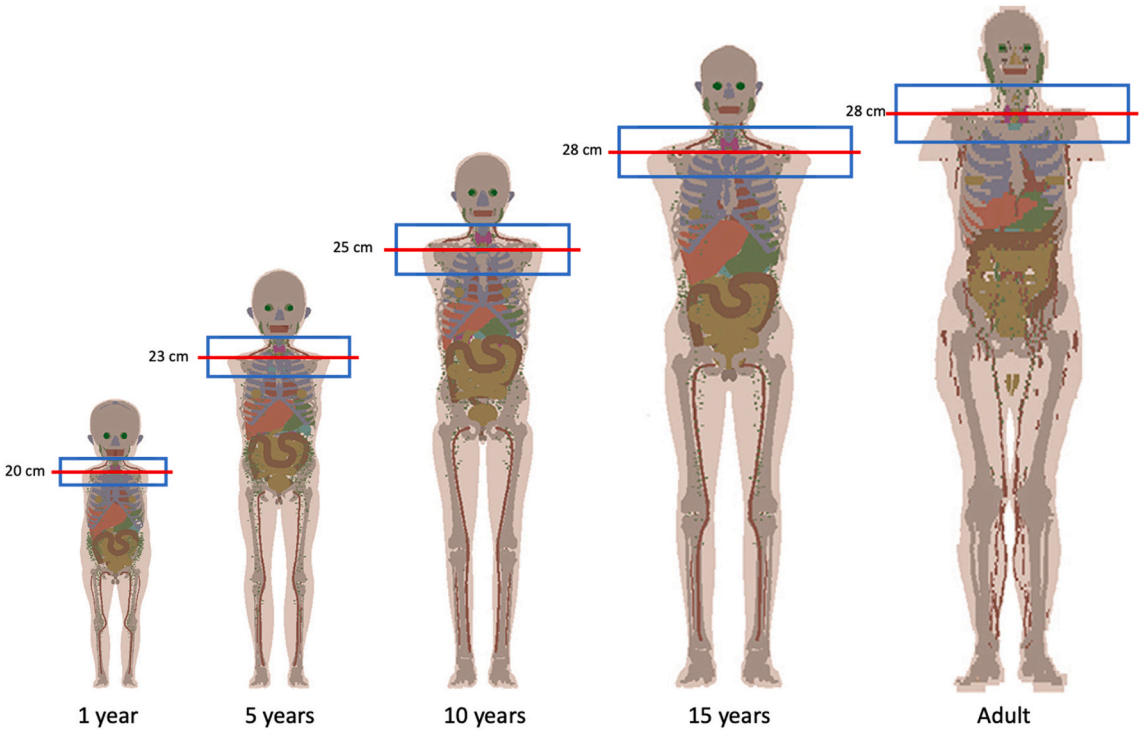

Fig. 1. The age-dependent computational human phantoms utilized in the NCICT program for organ dose calculations in this study. The locations of scan start for chest CT are represented by the red line on each phantom with the distance from the top of the phantom's head specified in cm on the left. The range of scan start locations used for random sampling is depicted by blue boxes.

2 = pediatric male, 3 = adult female, 4 = adult male), the height (cm) and weight (kg) of a patient, tube potential (kV), tube current modulation strength (0–1), the phantom type (1 = 16 cm, 2 = 32 cm) for $CTDI_{vol}$, and $CTDI_{vol}$ (mGy). For the current study, we adopted five computational human phantoms representing 1-, 5-, 10-, 15-year-old, and adult males since we wanted to focus on gender-neutral organs in the current study (Fig. 1). The only gender-specific tissue receving measurable doses would be the breast. However, it is always fully covered by chest CT which may not show substantial difference between males and females. Below the age of 15 years, pediatric breast models exhibit identical characteristics across genders. Since the height and weight distribution of COVID-19-related CT patients are not reported, we evaluated radiation dose to patients representing reference height and weight defined by the International Commission on Radiological Protection (ICRP). The tube potential of 120 kV was assumed for both pediatric and adult patients.

Using these parameters, NCICT calculates organ doses according to the following equation:

$$D_{organ} = \sum_{z=SS}^{z=SE} \frac{D_{MC}(organ, phantom, spectrum, z)}{CTDI_{vol,MC}(spectrum, CTDI\ phantom, z)} \times CTDI_{vol}(spectrum, CTDI\ phantom, z) \quad (2)$$

where z is the slice number ranging from 1 to the total number of slices with 1 cm interval, *phantom* is selected based on the parameters described above (phantom group number, height, and weight), *SS* and *SE* are the slice numbers at the scan start and end, respectively, described above, $D_{MC}(organ, phantom, spectrum, z)$ (mGy/photon) is organ dose per photon history pre-calculated from Monte Carlo simulation of the phantoms combined with CT x-ray source models, $CTDI_{vol,MC}$ (mGy/photon) is the $CTDI_{vol}$ per photon history calculated from the Monte Carlo simulation of CTDI phantoms (16 cm and 32 cm) coupled with CT x-ray models, and $CTDI_{vol}(spectrum, CTDI\ phantom, z)$ was provided from the literature review described above.

2.4. Plausible dose realizations

To evaluate the distribution of plausible organ doses and effective doses delivered to patients who underwent COVID-19-related chest CT scans worldwide, we adopted an uncertainty propagation method (Simon et al., 2015). We simulated 1000 sets of $CTDI_{vol}$ and scan coverage by randomly sampling from the PDFs of $CTDI_{vol}$ and scan start location created as described above. We utilized INDEX combined with RANDBETWEEN functions in Microsoft Excel to randomly sample $CTDI_{vol,sample}$ from its PDFs for standard dose and low dose protocols, and RANDBETWEEN function for sampling $Scan\ start_{sample}$ from the PDFs of scan start range as follows:

$$CTDI_{vol,sample} = INDEX(CTDI_{vol}\ array, RANDBETWEEN(1, arraysize)) \quad (3)$$

$$Scan\ start_{sample} = RANDBETWEEN(upper\ limit, lower\ limit) \quad (4)$$

where $CTDI_{vol}$ *array* is the array of $CTDI_{vol}$ values for standard and low dose protocols, *arraysize* is the length of the $CTDI_{vol}$ *array*, *upper limit* is the upper limit of scan start (e.g., 28 cm–8.8 cm = 19.2 cm for adult male), *lower limit* is the lower limit of scan start (e.g., 28 cm + 8.8 cm = 36.8 cm for adult male). The upper and lower limits of scan coverage are presented in Fig. 1 as blue boxes on each phantom. Once scan start

location was sampled, we added the average scan length obtained from literature to derive scan end location.

We created a total of 1000 sets of input lines for the NCICT program, distinguishing between standard (500 input lines) and low dose (500 input lines) protocols. Subsequently, employing the batch calculation feature of NCICT, we automated the computation of 1000 sets (500 for standard dose protocol and 500 for low dose protocol) of plausible doses, encompassing a total of 33 radiosensitive organs and tissues, including the lungs, stomach, colon, and active marrow (with a tissue weighting factor of 0.12 (ICRP, 2007)). Additionally, NCICT facilitated the derivation of an effective dose based on organ and tissue doses combined with tissue weighting factors.

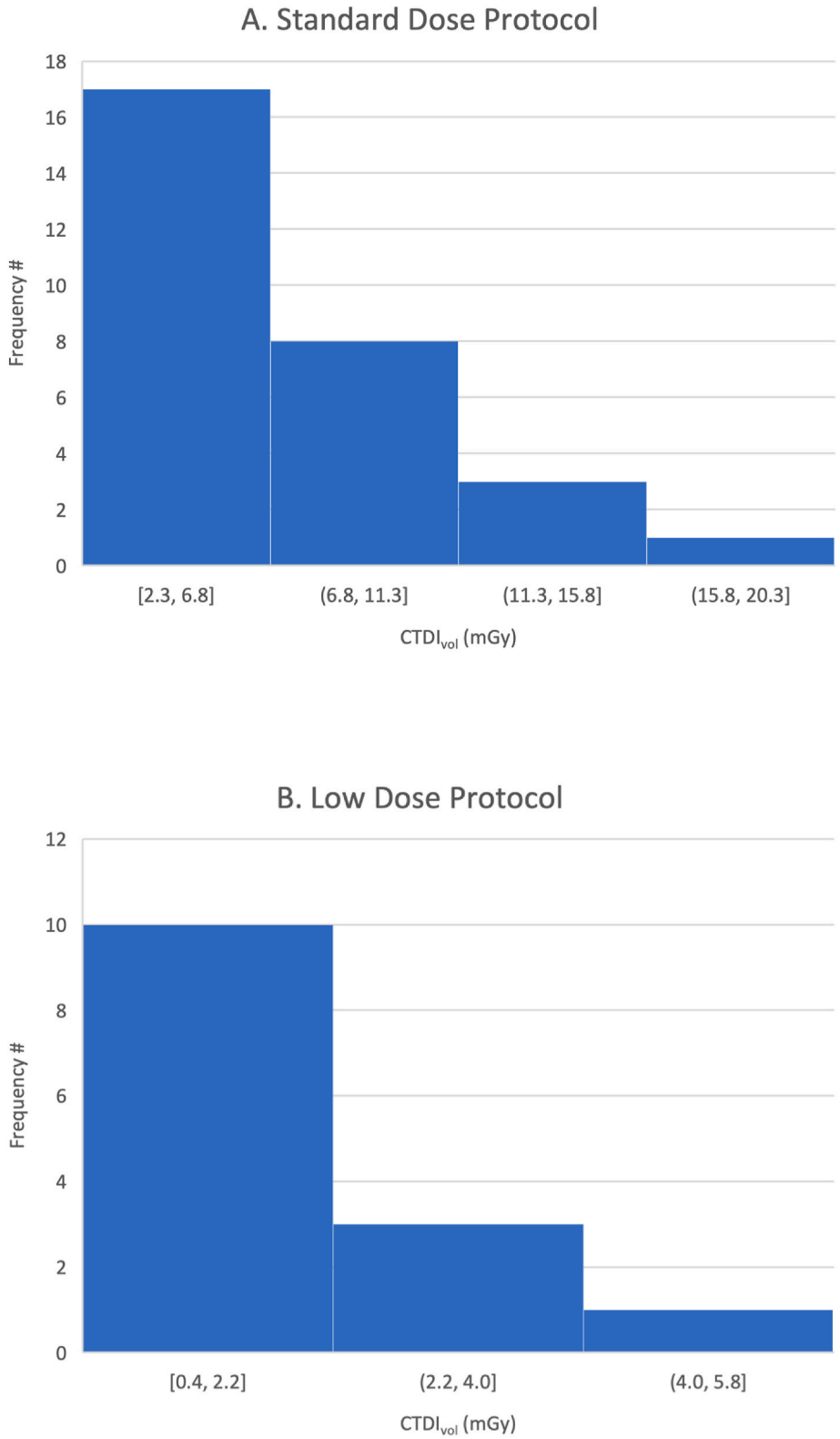

Fig. 2. Distribution of CTDIvol (mGy) for (a) standard dose and (b) low dose protocols collected from the literature.

Table 1A
Summary of dosimetric characteristics of CT scans conducted for COVID19 patients in different countries using **standard dose protocol**. Derived $CTDI_{vol}$ and DLP are presented in bold italics. Countries are italicized in bold when standard dose protocol was assumed based on $CTDI_{vol}$. Min, Q1, median, Q3, max, and median absolute deviation (MAD) values were calculated for $CTDI_{vol}$, DLP, and scan length.

Country	$CTDI_{vol}$ (mGy)				DLP (mGy-cm)				Scan Length (cm)	Reference
	Mean	SD	Min	Max	Mean	SD	Min	Max		
Belgium	***14.4***				520.0		310	906		(De Smet et al., 2021)
China	10.5		0.6	33.8	355.0		6.8	1098	34	(Zhou, 2020)
China	3.4				129.1				38	(Kang et al., 2020)
China	11.2	1.5			360.5	52.99			32	(Li et al., 2020)
China	8.4	2	5.2	12.6	***302.4***					(Pan et al., 2020)
China	***12.6***				454.7					(Wu et al., 2020)
China	4.1	0.9	2.3	5.8	***147.6***					(D. Liu et al., 2020)
China	6.2				***208.5***					(J. Liu et al., 2020)
China	9.3	4.1			314.0	152.8			34	(Wen et al., 2020)
National Median	8.9				308.24					
France	2.8		2.2	3.5	118.6		92	156	43	(Greffier et al., 2021)
France	***4.4***				160.0	40	80	400	36	(Herpe et al., 2021)
National Median	3.6				139.3					
Iran	13.2	2.5			412.8	91.7			31	(Tabatabaei et al., 2020b)
Iran	5.1		3.8	7.8	***183.6***					(Tabatabaei et al., 2020a)
Iran	4.9		3.9	7.8	***176.4***					(Tabatabaei et al., 2020c)
Iran	5.4		2.3	8.4	***192.6***					(Moradi et al., 2020)
National Median	5.2				188.1					
Italy	6.4		3.9	7.5	***226.2***		176	322		(Agostini et al., 2020)
Italy	6.8	2.7			239.0	94			35	(Ghetti et al., 2020)
Italy	8.9	1.6			334.2	33.8			38	(Falaschi et al., 2020)
Italy	15.1	2.4			557.6	62.6			37	(Falaschi et al., 2020)
National Median	7.9				286.6					
Saudi Arabia	4.8				***172.4***					(Saeed et al., 2023)
Saudi Arabia	2.3				***81.4***					(Saeed et al., 2023)
Saudi Arabia	5.3				***191.5***					(Saeed et al., 2023)
Saudi Arabia	3.0				***108.4***					(Saeed et al., 2023)
Saudi Arabia	5.2				***186.1***					(Saeed et al., 2023)
National Median	4.8				172.4					
Turkey	***7.2***				260.0					(Aslan et al., 2021)
Turkey	8.0				330.0				41	(Atlı et al., 2022)
Turkey	***5.3***				190.0		98	494		(Karakaş et al., 2021)
National Median	7.2				260.0					
Europe + USA	5.3	1.4	2.5	7.9	182.4	34.2	76.6	286.1	34	(Booz et al., 2021)
Min	2.3				81.4				31.3	
Q1	4.9				172.4				33.8	
Median (MAD)	5.8	(2.0)			200.5	(65.5)			36.0	(3.4)
Q3	9.0				330.0				37.6	
Max	15.1				557.6				42.5	

3. Results

Fig. 2 shows the distribution of CTDIvol values for standard and low dose protocols that were used to create 1000 realizations of CTDIvol for organ dose calculations. The $CTDI_{vol}$ and DLP with mean, standard deviation, min, and max by article are summarized for standard dose protocol (Table 1a) and low dose protocol (Table 1b). National median values were calculated and provided at the end of the country-specific data. For standard dose protocol (Table 1a), median $CTDI_{vol}$ ranges from 3.6 mGy (France) to 14.4 mGy (Belgium) although only a single data point was available for Belgium. Across the countries included in our study, the median of the mean $CTDI_{vol}$ and DLP values was 5.8 mGy and 200.5 mGy-cm, respectively. As for the low dose protocol (Table 1b), the lowest national $CTDI_{vol}$ is observed for France (0.4 mGy) with Turkey and Italy, the next lowest $CTDI_{vol}$, 0.6 mGy. The greatest low dose protocol $CTDI_{vol}$ is observed for Iran, which reports the $CTDI_{vol}$ of 3.5 mGy, which was proposed as a low-dose chest CT protocol (Agostini et al., 2020). Median of the mean $CTDI_{vol}$ and DLP values for low dose protocols are 1.1 mGy and 40.3 mGy-cm, respectively. The standard dose protocol administered approximately five times higher $CTDI_{vol}$ (5.8 mGy) to patients undergoing COVID-19-related chest CT scans compared to the low dose protocol (1.1 mGy).

A total of 1000 sets of organ doses (33 organs and tissues) and effective doses were calculated using the NCICT program where 1000 sets of batch input files were inputted. The full sets of doses are provided in the supplementary material. The five-number summary tables for 500 plausible organ and effective doses were provided for standard dose protocol (Table 2a) and low dose protocol (Table 2b). For both standard dose and low dose protocols, the lungs received the greatest dose out of the four organs while the colon received the smallest dose for all ages. For both protocols, the median lung dose (11.8 mGy) for the 1-year-old patients was about 1.5 times greater than that (7.8 mGy) of the adult patients. Median effective dose for 1-year-old patients was 1.2 and 1.1 times greater than the adult patients for standard dose and low dose protocols, respectively. 75% of whole COVID-19-related CT patients would have received effective doses less than 6.4 mSv and 1.5 mSv when scanned by standard dose and low dose protocols, respectively. However, maximum effective doses were up to 15.6 mSv (standard dose

Table 1B
Summary of dosimetric characteristics of CT scans conducted for COVID19 patients in different countries using **low dose protocol**. Countries are italicized in bold when low dose protocol was assumed based on $CTDI_{vol}$. Derived $CTDI_{vol}$ and DLP are presented in bold italics. Min, Q1, median, Q3, max, and median absolute deviation (MAD) values were calculated for $CTDI_{vol}$, DLP, and scan length.

Country	CTDIvol (mGy)				DLP (mGy-cm)				Scan Length (cm)	Reference
	Mean	SD	Min	Max	Mean	SD	Min	Max		
Belgium	1.3	0.59			39.9	17.8			31	Dangis et al. (2020)
China	4.4				159.4				36	Zhou (2020)
China	0.4				14.5				37	Kang et al. (2020)
China	2.5	0.27			87.3	10.21			34	Li et al. (2020)
China	2.4	1.11			93.9	45.6			39	Hu et al. (2020)
National Median	2.5				87.1					
Egypt	1.6	0.4			61.0	9.5			38	Samir et al. (2021)
Egypt	1.1	0.3			42.0	7.9			38	Samir et al. (2021)
National Median	1.4				51.5					
France	0.4		0.39	0.4	14.2		13.1	15.4	36	Greffier et al. (2021)
Germany	0.9	0.3			35.0	10.2			39	Hamper et al. (2020)
Germany	2.8	0.9			89.3	27.7			32	Steuwe et al. (2020)
National Median	1.9				62.2					
Iran	3.5	0.8			112.0	26.6			32	Tabatabaei et al. (2020b)
Italy	0.6		0.47	1.12	19.5		17.5	29	30	Agostini et al. (2020)
Turkey	***0.6***				20.4					Aslan et al. (2021)
Turkey	1.0				40.3				40	Atlı et al. (2022)
Turkey	***0.4***				15.6		12	32		Karakaş et al. (2021)
National Median	0.6				25.4					
Min	0.4				14.2				30.5	
Q1	0.6				19.7				32.0	
Median (MAD)	1.1	(0.7)			40.3	(24.7)			35.8	(3.3)
Q3	2.3				80.7				38.1	
Max	4.4				153.4				40.3	

Table 2A
Five-number summary of 500 plausible major organ doses (mGy) and effective doses (mSv) for patients with different age groups scanned by standard dose protocol.

Standard dose protocol		Lungs	Stomach	Colon	Active marrow	E (mSv)
1 years	Min	4.1	0.5	0.1	1.2	1.7
	Q1	10.0	2.6	0.2	2.8	4.1
	Median	11.8	4.7	0.4	3.4	5.0
	Q3	18.0	7.1	0.6	5.1	7.8
	Max	35.3	22.5	2.1	10.1	15.6
5 years	Min	2.1	0.9	0.1	0.6	1.7
	Q1	6.2	3.9	0.4	1.5	4.0
	Median	9.0	7.1	0.8	1.9	4.6
	Q3	14.0	10.5	1.8	3.0	7.2
	Max	29.8	29.2	13.3	6.2	14.4
10 years	Min	2.6	0.6	0.1	0.7	1.5
	Q1	6.5	2.7	0.3	1.7	3.5
	Median	8.7	5.8	0.7	2.1	4.4
	Q3	13.2	9.3	1.9	3.3	6.8
	Max	28.0	25.7	10.7	6.7	13.8
15 years	Min	2.5	0.2	0.0	0.7	0.9
	Q1	6.2	0.9	0.1	1.7	2.5
	Median	8.0	2.4	0.2	2.1	3.4
	Q3	12.3	5.4	0.4	3.2	5.2
	Max	25.9	21.8	2.7	6.6	12.0
30 years	Min	2.4	0.7	0.1	0.8	1.3
	Q1	5.6	3.5	0.3	1.8	3.1
	Median	7.8	5.8	0.8	2.3	4.2
	Q3	11.4	9.7	2.4	3.5	6.4
	Max	22.2	21.8	13.2	6.6	12.4

Table 2B
Five-number summary of 500 plausible major organ doses (mGy) and effective doses (mSv) for patients with different age groups scanned by low dose protocol.

Low dose protocol		Lungs	Stomach	Colon	Active marrow	E (mSv)
1 years	Min	0.30	0.03	0.00	0.08	0.08
	Q1	1.02	0.22	0.02	0.31	0.42
	Median	1.98	0.70	0.07	0.56	0.81
	Q3	4.54	1.80	0.20	1.25	1.80
	Max	10.06	8.63	2.05	3.61	5.72
5 years	Min	0.19	0.03	0.00	0.02	0.05
	Q1	0.90	0.56	0.05	0.19	0.47
	Median	1.67	1.13	0.18	0.35	0.84
	Q3	3.02	2.09	0.67	0.68	1.61
	Max	8.34	8.13	6.16	2.26	5.53
10 years	Min	0.31	0.04	0.00	0.05	0.11
	Q1	0.86	0.36	0.04	0.20	0.42
	Median	1.60	0.89	0.17	0.38	0.81
	Q3	3.57	2.00	0.54	0.83	1.65
	Max	7.75	7.51	5.03	2.33	4.88
15 years	Min	0.33	0.02	0.00	0.07	0.08
	Q1	0.86	0.16	0.01	0.22	0.33
	Median	1.49	0.43	0.04	0.39	0.62
	Q3	3.38	1.10	0.10	0.82	1.21
	Max	7.23	6.08	1.15	2.31	4.05
30 years	Min	0.36	0.05	0.00	0.07	0.13
	Q1	0.81	0.48	0.04	0.24	0.40
	Median	1.36	0.86	0.18	0.41	0.74
	Q3	3.18	1.94	0.63	0.85	1.50
	Max	6.01	5.88	5.10	2.47	4.30

protocol) and 5.72 mSv (low dose protocol) for 1-year-old patients. As for adult patients, standard dose protocol delivered about 6-fold greater median lung doses (7.8 mGy vs. 1.4 mGy) and effective doses (0.7 mSv vs. 4.2 mSv) compared to low dose protocol.

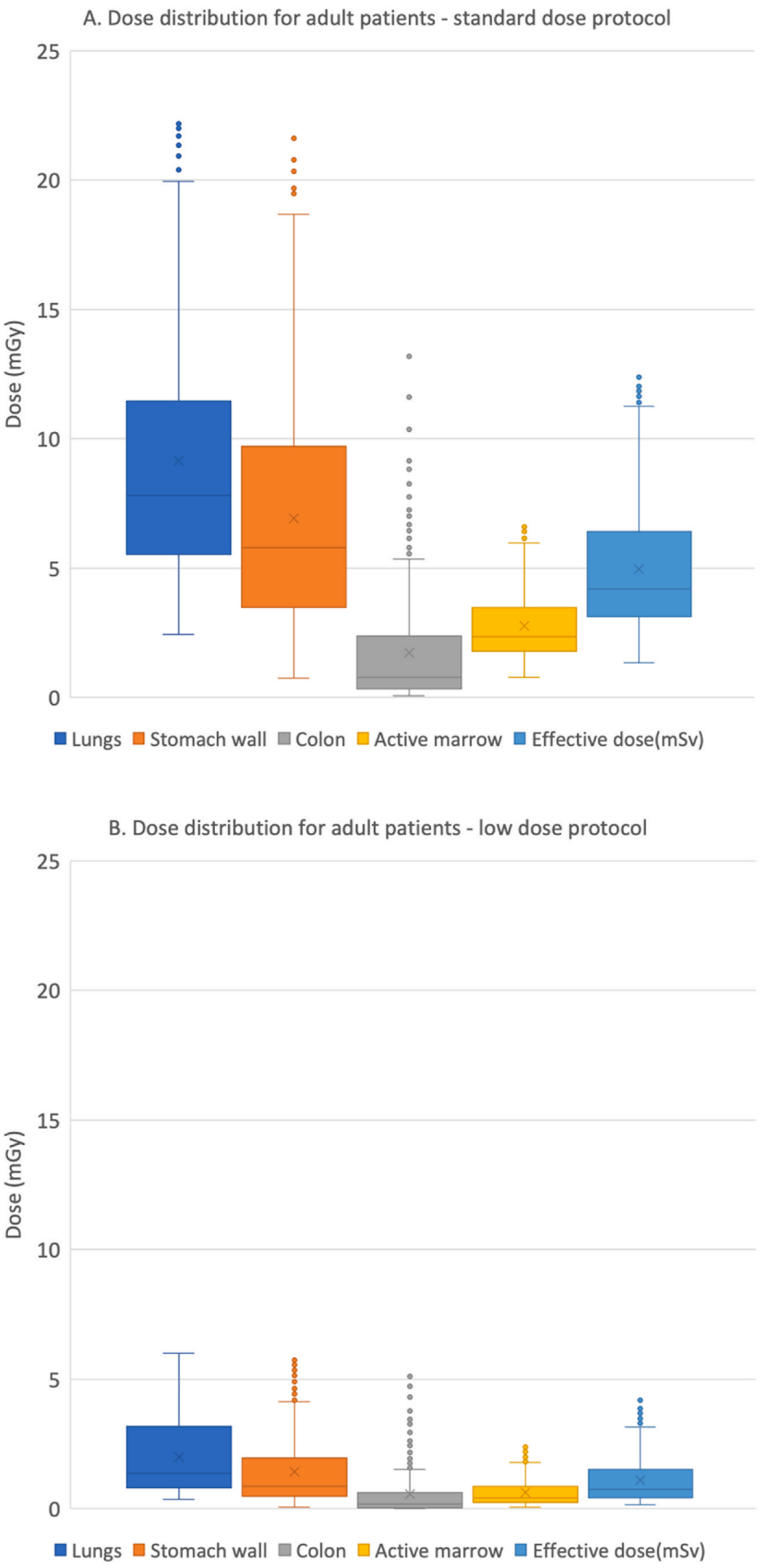

Fig. 3. Distribution of major organ doses and effective doses delivered to adult COVID19 chest CT patients scanned using (a) standard dose protocol (n = 500) and (b) low dose protocol (n = 500).

Fig. 3 shows the boxplot of the distribution of organ and effective doses of COVID19 adult patients undergoing chest CT scans by (a) standard dose protocol and (b) low dose protocol. It is clear that all doses are positively skewed (right-skewed). Interquartile ranges are quite different between the lungs and colon: 5.8 mGy for lungs and 2.0 for colon. For low dose protocol, the interquartile ranges are much smaller: 2.37 mGy for lungs and 0.59 for colon.

4. Discussion

Our study introduces an innovative approach to evaluating radiation dose distributions in chest CT scans for diagnosis of COVID-19 worldwide, focusing on a detailed examination of organ-specific doses—a facet that has not been extensively explored in previous research. While past studies have predominantly relied on major CT dose descriptors like $CTDI_{vol}$ and DLP, our work takes a step further. From literature, we identified two CT parameters impacting organ doses the most: CTDIvol and scan coverage (Dabin et al., 2016; Lee et al., 2019; McNitt-Gray, 2002). Through the generation of 1000 plausible CTDIvol and scan coverage and the utilization of the NCICT program, we pioneer the calculation of organ-specific doses for a diverse set of 33 radiosensitive organs and tissues. The results provide an in-depth understanding of how radiation is distributed within the body. Furthermore, we calculated effective dose directly from organ-specific doses not from DLP-to-effective dose conversion factors, which may lead to the errors up to 40% (Lee, 2020). Through the analysis of the plausible organ and effective dose data, we found that 75% of whole COVID-19-related CT patients would have received effective doses less than 6.4 mSv and 1.5 mSv when scanned by standard dose and low dose protocols, respectively.

We compared our effective doses with those from other data sources. National Council on Radiation Protection and Measurements reported the effective dose of 6.1 mSv for general chest CT based on American College of Radiology Dose Index Registry data and literature surveys (NCRP, 2019). This is comparable to our result, 6.4 mSv, for standard dose protocol. The NCRP also reports the effective dose of 0.1 mSv for chest radiography, which is substantially smaller than that from CT as expected. UNSCEAR also indicates effective dose of 6.4 mSv for thorax CT scans (UNSCEAR, 2022), which is identical to that from NCRP. Effective dose of 0.08 mSv is reported by UNSCEAR for thorax radiography.

This study, while contributing novel insights into organ-specific radiation doses in chest CT scans for COVID-19 patients, is subject to certain limitations that warrant consideration. Our use of the ICRP reference computational phantoms, instead of actual patient CT images, may be a noteworthy constraint. While these phantoms offer a standardized human anatomy, they may not fully encapsulate the anatomical diversity inherent in the COVID-19 patient population. The extent of organs and tissues encompassed in CT scan coverage may vary depending on an individual patient's anatomy, leading to significant differences in radiation dosage. Additionally, reliance on $CTDI_{vol}$ values from existing literature may introduce another limitation, as these values might not comprehensively represent the varied CT scan protocols adopted globally for COVID-19 patients. Variability in CTDIvol measurements may be noticeable within a single hospital setting and even among CT scanners that are identical. Finally, we categorized the findings by country and computed the median CTDIvol for each specific country. However, due to the variability in the number of hospitals and patients, the results specific to each country may not be fully representative. Given the evolving nature of imaging technologies, particularly in response to the pandemic, our findings should be interpreted with awareness of these constraints, emphasizing the need for future research to refine our understanding of organ-specific doses based on a broad collection of patient- and scan-specific electronic records.

5. Conclusion

We established comprehensive data of $CTDI_{vol}$ for the COVID-19-related chest CT scans by reviewing the literature. By using the data combined with the uncertainty propagation technique, we created a total of 1000 sets of plausible organ and effective doses. We found that pediatric patients received up to 1.5 times greater lung doses than adult patients and the vast majority of the patient population received effective doses less than 6.4 mSv even under standard dose protocol. While past studies have predominantly reported CT dose descriptors such as $CTDI_{vol}$ and DLP, our work takes it a step further by reporting organ-level doses and effective doses. Our discovery of a significant contrast in effective radiation dose between standard and low-dose protocols underscores the necessity of weighing diagnostic advantages against radiation exposure in CT examinations for forthcoming respiratory pandemic illnesses. Subsequent research endeavors could involve enhancing the precision of radiation dose assessment through the collection of a subset of electronic CT records. Longitudinal epidemiological studies could also be undertaken to monitor the long-term adverse health effects of such exposure on COVID-19 patients over time.

CRediT authorship contribution statement

Daniel Lee: Data curation, Formal analysis, Investigation, Methodology, Software, Validation, Writing – original draft, Conceptualization. **Jae Won Jung:** Conceptualization, Data curation, Formal analysis, Investigation, Methodology, Project administration, Resources, Software, Supervision, Validation, Visualization, Writing – review & editing.

Declaration of competing interest

The authors declare that they have no known competing financial interests or personal relationships that could have appeared to influence the work reported in this paper.

Data availability

Data will be made available on request.

References

Agostini, A., Floridi, C., Borgheresi, A., Badaloni, M., Esposto Pirani, P., Terilli, F., Ottaviani, L., Giovagnoni, A., 2020. Proposal of a low-dose, long-pitch, dual-source chest CT protocol on third-generation dual-source CT using a tin filter for spectral shaping at 100 kVp for CoronaVirus Disease 2019 (COVID-19) patients: a feasibility study. Radiol. Med. 125, 365–373. https://doi.org/10.1007/s11547-020-01179-x.

Aslan, S., Bekçi, T., Çakır, İ.M., Ekiz, M., Yavuz, İ., Şahin, A.M., 2021. Diagnostic performance of low-dose chest CT to detect COVID-19: a Turkish population study. Diagn. Interv. Radiol. Ank. Turk. 27, 181–187. https://doi.org/10.5152/dir.2020.20350.

Atlı, E., Uyanık, S.A., Öğüşlü, U., Cenkeri, H.Ç., Yılmaz, B., Gümüş, B., 2022. The feasibility of low-dose chest CT acquisition protocol for the imaging of COVID-19 pneumonia. Curr. Med. Imaging 18, 38–44. https://doi.org/10.2174/1573405617666210623124108.

Booz, C., Vogl, T.J., Joseph Schoepf, U., Caruso, D., Inserra, M.C., Yel, I., Martin, S.S., Bucher, A.M., Lenga, L., Caudo, D., Schreckenbach, T., Schoell, N., Huegel, C., Stratmann, J., Vasa-Nicotera, M., Rachovitsky-Duarte, D.E., Laghi, A., De Santis, D., Mazziotti, S., D'Angelo, T., Albrecht, M.H., 2021. Value of minimum intensity projections for chest CT in COVID-19 patients. Eur. J. Radiol. 135, 109478 https://doi.org/10.1016/j.ejrad.2020.109478.

Bosch De Basea Gomez, M., Thierry-Chef, I., Harbron, R., Hauptmann, M., Byrnes, G., Bernier, M.-O., Le Cornet, L., Dabin, J., Ferro, G., Istad, T.S., Jahnen, A., Lee, C., Maccia, C., Malchair, F., Olerud, H., Simon, S.L., Figuerola, J., Peiro, A., Engels, H., Johansen, C., Blettner, M., Kaijser, M., Kjaerheim, K., Berrington De Gonzalez, A., Journy, N., Meulepas, J.M., Moissonnier, M., Nordenskjold, A., Pokora, R., Ronckers, C., Schüz, J., Kesminiene, A., Cardis, E., 2023. Risk of hematological malignancies from CT radiation exposure in children, adolescents and young adults. Nat. Med. https://doi.org/10.1038/s41591-023-02620-0.

Dabin, J., Mencarelli, A., McMillan, D., Romanyukha, A., Struelens, L., Lee, C., 2016. Validation of calculation algorithms for organ doses in CT by measurements on a 5 year old paediatric phantom. Phys. Med. Biol. 61, 4168–4182. https://doi.org/10.1088/0031-9155/61/11/4168.

Dangis, A., Gieraerts, C., De Bruecker, Y., Janssen, L., Valgaeren, H., Obbels, D., Gillis, M., Van Ranst, M., Frans, J., Demeyere, A., Symons, R., 2020. Accuracy and reproducibility of low-dose submillisievert chest CT for the diagnosis of COVID-19. Radiol. Cardiothorac. Imaging 2, e200196. https://doi.org/10.1148/ryct.2020200196.

De Smet, K., De Smet, D., Ryckaert, T., Laridon, E., Heremans, B., Vandenbulcke, R., Demedts, I., Bouckaert, B., Gryspeerdt, S., Martens, G.A., 1 january 2021. Diagnostic performance of chest CT for SARS-CoV-2 infection in individuals with or without COVID-19 symptoms. Radiology 298 (1), E30–37. https://doi.org/10.1148/radiol.2020202708.

Falaschi, Z., Danna, P.S.C., Arioli, R., Pasché, A., Zagaria, D., Percivale, I., Tricca, S., Barini, M., Aquilini, F., Andreoni, S., Carriero, A., 2020. Chest CT accuracy in diagnosing COVID-19 during the peak of the Italian epidemic: a retrospective correlation with RT-PCR testing and analysis of discordant cases. Eur. J. Radiol. 130, 109192 https://doi.org/10.1016/j.ejrad.2020.109192.

Ghetti, C., Ortenzia, O., Maddalo, M., Altabella, L., Sverzellati, N., 2020. Dosimetric and radiation cancer risk evaluation of high resolution thorax CT during COVID-19 outbreak. Phys. Medica PM Int. J. Devoted Appl. Phys. Med. Biol. Off. J. Ital. Assoc. Biomed. Phys. AIFB 80, 119–124. https://doi.org/10.1016/j.ejmp.2020.10.018.

Goo, H.W., 2012. CT radiation dose optimization and estimation: an update for radiologists. Korean J. Radiol. 13, 1–11. https://doi.org/10.3348/kjr.2012.13.1.1.

Greffier, J., Hoballah, A., Sadate, A., de Oliveira, F., Claret, P.-G., de Forges, H., Loubet, P., Mauboussin, J.-M., Hamard, A., Beregi, J.-P., Frandon, J., 2021. Ultra-low-dose chest CT performance for the detection of viral pneumonia patterns during the COVID-19 outbreak period: a monocentric experience. Quant. Imag. Med. Surg. 11, 3190–3199. https://doi.org/10.21037/qims-20-1176.

Hamper, C.M., Fleckenstein, F.N., Büttner, L., Hamm, B., Thieme, N., Thiess, H.-M., Scholz, O., Döllinger, F., Böning, G., 2020. Submillisievert chest CT in patients with COVID-19 - experiences of a German Level-I center. Eur. J. Radiol. Open 7, 100283. https://doi.org/10.1016/j.ejro.2020.100283.

Hauptmann, M., Byrnes, G., Cardis, E., Bernier, M.-O., Blettner, M., Dabin, J., Engels, H., Istad, T.S., Johansen, C., Kaijser, M., Kjaerheim, K., Journy, N., Meulepas, J.M., Moissonnier, M., Ronckers, C., Thierry-Chef, I., Le Cornet, L., Jahnen, A., Pokora, R., Bosch de Basea, M., Figuerola, J., Maccia, C., Nordenskjold, A., Harbron, R.W., Lee, C., Simon, S.L., Berrington de Gonzalez, A., Schüz, J., Kesminiene, A., 2023. Brain cancer after radiation exposure from CT examinations of children and young adults: results from the EPI-CT cohort study. Lancet Oncol. 24, 45–53. https://doi.org/10.1016/S1470-2045(22)00655-6.

Herpe, G., Lederlin, M., Naudin, M., Ohana, M., Chaumoitre, K., Gregory, J., Vilgrain, V., Freitag, C.A., De Margerie-Mellon, C., Flory, V., Ludwig, M., Mondot, L., Fitton, I., Jacquier, A.R.R., Ardilouze, P., Petit, I., Gervaise, A., Bayle, O., Crombe, A., Mekuko Sokeng, M., Thomas, C., Henry, G., Bliah, V., Le Tat, T., Guillot, M.-S., Gendrin, P., Garetier, M., Bertolle, E., Montagne, C., Langlet, B., Kalaaji, A., Kayayan, H., Desmots, F., Dhaene, B., Saulnier, P.-J., Guillevin, R., Bartoli, J.-M., Beregi, J.-P., Tasu, J.P., 2021. Efficacy of chest CT for COVID-19 pneumonia diagnosis in France. Radiology 298, E81–E87. https://doi.org/10.1148/radiol.2020202568.

Homayounieh, F., Holmberg, O., Al Umairi, R., Aly, S., Basevičius, A., Costa, P.R., Darweesh, A., Gershan, V., Ilves, P., Kostova-Lefterova, D., Renha, S.K., Mohseni, I., Rampado, O., Rotaru, N., Shirazu, I., Sinitsyn, V., Turk, T., Van Ngoc Ty, C., Kalra, M.K., Vassileva, J., 2020. Variations in CT utilization, protocols, and radiation doses in COVID-19 pneumonia: results from 28 countries in the IAEA study. Radiology 203453. https://doi.org/10.1148/radiol.2020203453.

Hu, Q., Guan, H., Sun, Z., Huang, L., Chen, C., Ai, T., Pan, Y., Xia, L., 2020. Early CT features and temporal lung changes in COVID-19 pneumonia in Wuhan, China. Eur. J. Radiol. 128, 109017 https://doi.org/10.1016/j.ejrad.2020.109017.

ICRP, 2020. Paediatric Reference Computational Phantoms. ICRP Publ. 143 Ann ICRP.

ICRP, 2010. Adult reference computational phantoms. ICRP Publ. 110 Ann ICRP 39.

ICRP, 2007. The 2007 Recommendations of the International Commission on Radiological Protection, vol. 37. ICRP Publ. 103 Ann ICRP, pp. 1–332.

Kang, Z., Li, X., Zhou, S., 2020. Recommendation of low-dose CT in the detection and management of COVID-2019. Eur. Radiol. 30, 4356–4357. https://doi.org/10.1007/s00330-020-06809-6.

Karakaş, H.M., Yıldırım, G., Çiçek, E.D., 2021. The reliability of low-dose chest CT for the initial imaging of COVID-19: comparison of structured findings, categorical diagnoses and dose levels. Diagn. Interv. Radiol. Ank. Turk. 27, 607–614. https://doi.org/10.5152/dir.2021.20802.

Lee, C., 2020. How to estimate effective dose for CT patients. Eur. Radiol. s00330-019-06625–7. https://doi.org/10.1007/s00330-019-06625-7.

Lee, C., Kim, K.P., Bolch, W.E., Moroz, B.E., Folio, Les, 2015. NCICT: a computational solution to estimate organ doses for pediatric and adult patients undergoing CT scans. J. Radiol. Prot. 35, 891–909. https://doi.org/10.1088/0952-4746/35/4/891.

Lee, C., Kuzmin, G.A., Bae, J., Yao, J., Mosher, E., Folio, L.R., 2019. Automatic mapping of CT scan locations on computational human phantoms for organ dose estimation. J. Digit. Imag. 32, 175–182. https://doi.org/10.1007/s10278-018-0119-2.

Lee, C., Yeom, Y.S., Folio, L., 2022. CT organ dose calculator size adaptive for pediatric and adult patients. Biomed. Phys. Eng. Express 8, 065020. https://doi.org/10.1088/2057-1976/ac9845.

Li, J., Wang, X., Huang, X., Chen, F., Zhang, X., Liu, Y., Luo, G., Xu, X., 2020. Application of CareDose 4D combined with Karl 3D technology in the low dose computed tomography for the follow-up of COVID-19. BMC Med. Imag. 20, 56. https://doi.org/10.1186/s12880-020-00456-5.

Liu, D., Li, L., Wu, X., Zheng, D., Wang, J., Yang, L., Zheng, C., 2020. Pregnancy and perinatal outcomes of women with coronavirus disease (COVID-19) pneumonia: a preliminary analysis. AJR Am. J. Roentgenol. 215, 127–132. https://doi.org/10.2214/AJR.20.23072.

Liu, J., Chen, T., Yang, H., Cai, Y., Yu, Q., Chen, J., Chen, Z., Shang, Q.-L., Ma, C., Chen, X., Xiao, E., 2020. Clinical and radiological changes of hospitalised patients with COVID-19 pneumonia from disease onset to acute exacerbation: a multicentre paired cohort study. Eur. Radiol. 30, 5702–5708. https://doi.org/10.1007/s00330-020-06916-4.

McNitt-Gray, M.F., 2002. AAPM/RSNA physics tutorial for residents: topics in CT. Radiographics 22, 1541.

Moradi, B., Ghanaati, H., Kazemi, M.A., Gity, M., Hashemi, H., Davari-Tanha, F., Chavoshi, M., Rouzrokh, P., Kolahdouzan, K., 2020. Implications of sex difference in CT scan findings and outcome of patients with COVID-19 pneumonia. Radiol. Cardiothorac. Imaging 2, e200248. https://doi.org/10.1148/ryct.2020200248.

NCRP, 2019. Medical Radiation Exposure of Patients in the United States. No. Report No. 184).

Pan, F., Ye, T., Sun, P., Gui, S., Liang, B., Li, L., Zheng, D., Wang, J., Hesketh, R.L., Yang, L., Zheng, C., 2020. Time course of lung changes at chest CT during recovery from coronavirus disease 2019 (COVID-19). Radiology 295, 715–721. https://doi.org/10.1148/radiol.2020200370.

Pearce, M.S., Salotti, J.A., Little, M.P., McHugh, K., Lee, C., Kim, K.P., Howe, N.L., Ronckers, C.M., Rajaraman, P., Sir Craft, A.W., Parker, L., Berrington de González, A., 2012. Radiation exposure from CT scans in childhood and subsequent risk of leukaemia and brain tumours: a retrospective cohort study. Lancet 380, 499–505. https://doi.org/10.1016/S0140-6736(12)60815-0.

Saeed, M.K., Alshamrani, H.A., Abdullah, Y.M., Ali, A.S.A.M., Almalki, Y., Alqfail, K.A., 2023. Chest CT utilization in COVID-19: a dosimetric and diagnostic-quality study. Radiat. Prot. Dosimetry ncad174. https://doi.org/10.1093/rpd/ncad174.

Samir, A., El-Husseiny, R.M., Sweed, R.A., El-Maaboud, N.A.E.-M.A., Masoud, M., 2021. Ultra-low-dose chest CT protocol during the second wave of COVID-19 pandemic: a double-observer prospective study on 250 patients to evaluate its detection accuracy. Egypt. J. Radiol. Nucl. Med. 52, 136. https://doi.org/10.1186/s43055-021-00512-2.

Simon, S.L., Hoffman, F.O., Hofer, E., 2015. The two-dimensional Monte Carlo: a new methodologic paradigm for dose reconstruction for epidemiological studies. Radiat. Res. 183, 27–41. https://doi.org/10.1667/RR13729.1.

Steuwe, A., Rademacher, C., Valentin, B., Köhler, M.-H., Appel, E., Keitel, V., Timm, J., Antoch, G., Aissa, J., 2020. Dose-optimised chest computed tomography for diagnosis of Coronavirus Disease 2019 (COVID-19) - evaluation of image quality and diagnostic impact. J. Radiol. Prot. Off. J. Soc. Radiol. Prot. 40, 877–891. https://doi.org/10.1088/1361-6498/aba16a.

Tabatabaei, S.M.H., Rahimi, H., Moghaddas, F., Rajebi, H., 2020a. Predictive value of CT in the short-term mortality of Coronavirus Disease 2019 (COVID-19) pneumonia in nonelderly patients: a case-control study. Eur. J. Radiol. 132, 109298 https://doi.org/10.1016/j.ejrad.2020.109298.

Tabatabaei, S.M.H., Talari, H., Gholamrezanezhad, A., Farhood, B., Rahimi, H., Razzaghi, R., Mehri, N., Rajebi, H., 2020b. A low-dose chest CT protocol for the diagnosis of COVID-19 pneumonia: a prospective study. Emerg. Radiol. 27, 607–615. https://doi.org/10.1007/s10140-020-01838-6.

Tabatabaei, S.M.H., Talari, H., Moghaddas, F., Rajebi, H., 2020c. CT features and short-term prognosis of COVID-19 pneumonia: a single-center study from kashan, Iran. Radiol. Cardiothorac. Imaging 2, e200130. https://doi.org/10.1148/ryct.2020200130.

UNSCEAR, 2022. SOURCES, EFFECTS AND RISKS OF IONIZING RADIATION (No. 2020/2021). United Nations Publications.

Wen, Z., Chi, Y., Zhang, L., Liu, H., Du, K., Li, Z., Chen, J., Cheng, L., Wang, D., 2020. Coronavirus disease 2019: initial detection on chest CT in a retrospective multicenter study of 103 Chinese subjects. Radiol. Cardiothorac. Imaging 2, e200092. https://doi.org/10.1148/ryct.2020200092.

Wu, J., Pan, J., Teng, D., Xu, X., Feng, J., Chen, Y.-C., 2020. Interpretation of CT signs of 2019 novel coronavirus (COVID-19) pneumonia. Eur. Radiol. 30, 5455–5462. https://doi.org/10.1007/s00330-020-06915-5.

Zhou, X., 2020. Automatic segmentation of multiple organs on 3D CT images by using deep learning approaches. Adv. Exp. Med. Biol. 1213, 135–147. https://doi.org/10.1007/978-3-030-33128-3_9.